Efficient Analysis Technique for Modeling Periodic Structures Based on Finite Element Method using High-Order Multiscalets Functions

Adel Ben Ali, El Amjed Hajlaoui, and Ali Gharsallah

Unité de Recherche Circuits et Systèmes d'Electronique Haute Fréquence, Département de physique
Faculté des sciences de Tunis, 2092 El Manar, Tunis. Tunisia
adel.benali@laposte.net, hajlamjed@yahoo.fr, ali.gharsallah@fst.rnu.tn

Abstract- Periodic structures have a variety of important applications in electromagnetic engineering and modern technologies. Commonly used, periodic structures include frequency selective surfaces, optical gratings, phased array antennas and various metamaterials. A three-dimensional finite element method (FEM) with efficient boundaries conditions is presented to simulate the electromagnetic properties of homogeneous periodic material. In our approach, we describe an accurate and efficient numerical analysis based on high-order multiscalets applied in vector edge FEM using new reduction meshing technique (MSRM-FEM) to characterize the electromagnetic properties of periodic structures. Here, we have achieved a factor of 4 in memory reduction and 7~11 in CPU speedup over the typical meshing. The FEM is applied to solve Maxwell's equation in the unit cell. The Floquet's theorem is used to take into account the periodicity of the boundaries conditions radiation for the unit cell. The numerical results are compared to published data and other simulation results. Good agreement is important to establish the validity and usefulness of the (MSRM-FEM) method given in this paper.

Index Terms- 3-D FEM, multiscalets functions, periodic structures, reduction meshing.

I. INTRODUCTION

Periodic structures are important in the analysis of electromagnetics scattering and radiation for various engineering applications. The periodicity in geometry is often exploited to achieve some desired electromagnetic proprieties. Many microwave and optical devices, such as frequency selective structures (FSS) [1] and phased array antennas [2], fall into this category.

Analysis of periodic structures has been carried out using a variety of numerical methods, such as the finite difference time domain (FDTD), the moment method (MoM), the finite element method (FEM), the transmission line method (TLM), and iterative methods [3].

Among these methods, FEM excels the modelling of complex homogeneous and inhomogeneous structures geometries. The FEM is, also, able to incorporate different types of boundaries and different excitation modes without significantly affecting its formulation. The FEM modelling of periodic structures has been reported in literature for both scattering [4] and radiation analysis [5].

In our approach, we propose multiscalets as basis functions to replace the traditional linear or higher order Lagrange, Hierarchical [6] interpolation shape functions in the finite-element formulation.

Since we employ multiscalets in our modelling, a brief review is given here. More detailed theory and background of multiscalets are presented in many references such as [7-8].

In this paper, we present a robust, higher-order multiscalets combined with FEM method [9] to model infinitely periodic array-structures, by imposing appropriate radiation boundaries conditions and periodic boundaries conditions. The computational domain is confined to a single unit cell of the infinite array. The unit cell interior region is discretized with regular tetrahedral element to model its geometry.

When the structures contain many unit cells, the structure extends to infinity in the periodic direction as illustrated in Fig. 1.

This purpose is to greatly simplify the electromagnetic analysis and minimize the CPU time of simulation by enabling the characterization of the electromagnetic interaction with the entire structure. Here, we will use a new strategy meshing for the regular design applied in microwave structures when we use the edge element formulation.

A new mesh-truncated technique is introduced for the frequency domain solution of closed and open region scattering problems

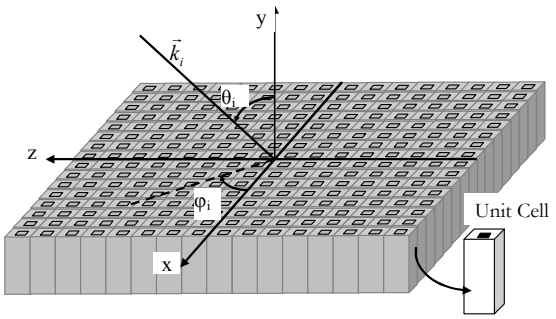

Fig. 1. Graphical representation of a plan wave incident on a generic 3-D periodic structure.

II. MULTISCALETS FUNCTIONS

Basic theory of orthogonal multiwavelets, multi-resolutions, and multiscalets can be found in many mathematical papers, e.g. [7] and [8].

The multiscalets $\phi_0(t)$, $\phi_1(t)\ldots\ \phi_{r-1}(t)$, are polynomials of degree $2r-1$ on [0, 1] and zero elsewhere, with $r-1$ continuous derivatives. In electromagnetics, the order is usually ≤ 4. They satisfy

$$\Phi(n) = \delta_{1,n} I, \tag{1}$$

where $\delta_{m,n}$ is the Kronecker delta, I is the identity matrix of size $r \times r$, r is the multiplicity coefficient, and

$$\Phi(t) = \begin{bmatrix} \phi_0(t) & \cdots & \phi_0^{(r-1)}(t) \\ \vdots & \ddots & \vdots \\ \phi_{r-1}(t) & \cdots & \phi_{r-1}^{(r-1)}(t) \end{bmatrix}. \tag{2}$$

The column vector

$$\varphi(t) = \left(\varphi_0(t)\ldots\varphi_{r-1}(t)\right)^T. \tag{3}$$

For all r, satisfies that $\phi_j(t) \neq 0$ only on two intervals [0, 1] and [1, 2]. The function values and its $(r-1)$ derivatives are specified at each integer edge. If $\varphi_j(t)$ is defined on [0, 2], then they are alternatively symmetric and anti-symmetric about $t = 1$.

The dilation equation may be written as

$$\begin{aligned} \phi(t) &= \sum_k C_k \phi(2t-k) \\ &= C_0\phi(2t) + C_1\phi(2t-1) + C_2\phi(2t-2) \end{aligned}. \tag{4}$$

Since the support is [0, 2], the only nonzero coefficients are C_0, C_1, and C_2, there are r basis functions at each edge, and C_i are matrices of $r \times r$ $(i = 0, 1, 2)$.

The polynomials of degree $2r-1$ on [0, 1] and [1, 2] are determined by:

$$\begin{aligned} &\left(\frac{d}{dt}\right)^k \phi_j(1) = \delta_{k,j}, && k, j = 0,\ldots,r-1 \\ &\left(\frac{d}{dt}\right)^k \phi_j(0) = \left(\frac{d}{dt}\right)^k \phi_j(2) = 0, && k, j = 0,\ldots,r-1 \end{aligned}. \tag{5}$$

From (1), we define

$$\phi(1) = \begin{bmatrix} \phi_0(1) & \phi_0^{(1)}(1) & \cdots & \phi_0^{(r-1)}(1) \\ \phi_1(1) & \phi_1^{(1)}(1) & \cdots & \phi_1^{(r-1)}(1) \\ \vdots & \vdots & \vdots & \vdots \\ \phi_{r-1}(1) & \phi_{r-1}^{(1)}(1) & \cdots & \phi_{r-1}^{(r-1)}(1) \end{bmatrix} = I. \tag{6}$$

Explicitly, it appears that ϕ_0(t) interpolates at the sampling point $t=1$, but assumes 0 at other sampling points $t=0$. The derivatives $\phi_0^{(k)}(t)$, k=1,2....,r-1 are zero at all integer sampling points. Similarly, interpolates at integer point, but assumes zero elsewhere for any derivatives other than 1.

In general,

$$\varphi_i^{(j)}(m) = \delta_{i,j}\delta_{1,m}, \quad i, j = 0,1,\ldots,r-1. \tag{7}$$

While spline interpolation fits a set of function values by solving a coupled linear system [8], the property (7) of the multiscalets provides interpolation that is completely uncoupled. Here, $\phi_i(t)$, $i=0,1....,r-1$ will be employed in the finite element as the shape functions.

The matrix coefficients in (4) can be derived by the following procedure:

$$\begin{aligned} C_0 &= \Phi\left(\frac{1}{2}\right)\Lambda, \\ C_1 &= \Phi(1)\Lambda = I\Lambda, \\ C_2 &= \Phi\left(\frac{3}{2}\right)\Lambda \end{aligned} \tag{8}$$

where

$$\Lambda = diag\left\{1, \frac{1}{2}, \left(\frac{1}{2}\right)^2, \ldots\ldots\ldots, \left(\frac{1}{2}\right)^{r-1}\right\}. \tag{9}$$

Matrices C_0 and C_2 related by

$$C_0 = SC_2S^{-1}, \tag{10}$$

with

$$S = S^{-1} = diag\left\{1,(-1),.....,(-1)^{r-1}\right\} . \tag{11}$$

The Matrix C_2 is given by

$$C_2 = U^{-1}\Gamma U \tag{12}$$

$$\Gamma = diag\left\{\left(\frac{1}{2}\right)^r,\left(\frac{1}{2}\right)^{r+1},.....,\left(\frac{1}{2}\right)^{2r-1}\right\} , \tag{13}$$

and

$$U_{mn} = (-1)^{r+m+n}\frac{(r+m-1)!}{(r+m-n)!}. \tag{14}$$

The multiscalets $\phi_0(t)$ and $\phi_1(t)$ are polynomials of degree $2r$-1 can be built by a simple iteration program or an eigenvalue algorithm called the cascade method from the dilatation matrices C_i [7]. In general multiscalets with arbitrary r have the form

$$\phi(t) = \begin{cases} \phi_0(t) = a_{1,1}t^{2r-1} + a_{1,2}t^{2r-2} + \cdots + a_{1,r}t^r \\ \cdots = \cdots \\ \cdots = \cdots \\ \phi_{r-1}(t) = a_{r,1}t^{2r-1} + a_{r,2}t^{2r-2} + \cdots + a_{r,r}t^r \end{cases}$$

$$\{\varphi\} = [A]\{T\}, \tag{15}$$

where the coefficient $a_{i,j}$ are obtained by inverting the matrix whose entries are

$$[\mathrm{B}] \Rightarrow b(i,j) = \frac{(2r-i)!}{(2r-i-j+1)!}, \quad i,j = 1,2,\ldots,r \tag{16}$$

where

$$[A] = [B]^{-1}. \tag{17}$$

It was found that for $r=2$,

$$t \in [0,1]\begin{cases}\phi_0(t) = 3t^2 - 2t^3 \\ \phi_1(t) = t^3 - t^2\end{cases} . \tag{18}$$

In case $r=3$, the explicit polynomial of $\phi_0(t)$, $\phi_1(t)$ and $\phi_2(t)$ are

$$\begin{cases}\phi_0(t) = 6t^5 - 15t^4 + 10t^3 \\ \phi_1(t) = -3t^5 + 7t^4 - 4t^3 \\ \phi_2(t) = \frac{1}{2}t^5 - t^4 + \frac{1}{2}t^3\end{cases} . \tag{19}$$

III. FEM FORMULATION

A. Discretization

The boundary value problem in the full-wave analysis of an inhomogeneous field waveguide is defined by the vector wave equation in the 3-D waveguide problem, [9, 10].

Maxwell's equations for the electromagnetic fields inside the computation domain are:

$$\begin{aligned}\nabla \times E &= -j\omega\mu_0\varepsilon_r H \\ \nabla \times H &= j\omega\mu_0\varepsilon_r E + J\end{aligned} . \tag{20}$$

Here, we eliminate H in the two equations above results in the wave equation for E:

$$\nabla \times \left(\frac{1}{\mu_r}\nabla \times E\right) - k_0^2\varepsilon_r E = -jk_0 Z_0 J . \tag{21}$$

Assuming that E satisfies some boundaries conditions on the surface S enclosing the computation domain Ω, it can be shown that the original problem is equivalent to the following variational problem

$$\delta F(E) = 0, \tag{22}$$

where

$$F(E) = \frac{1}{2}\iiint_V \left[\frac{1}{\mu_r}(\nabla \times E)\cdot(\nabla \times E) - k_0^2\varepsilon_r E\cdot E\right]d\Omega + jk_0 Z_0 \iiint_V E\cdot J\, d\Omega + Surface\ Integral\ Terms. \tag{23}$$

The surface integral terms are the results of corresponding boundaries conditions [11].

To solve the variational problem (23), the entire computation domain Ω is divided into small elements. In the FEM discretization, commonly used elements are tetrahedral elements for 3-D problems.

The next step involves expanding the electromagnetic fields in terms of basis functions in each element. In the context of 3-D problems, it is more convenient to use vector basis functions instead of scalar basis functions.

For tetrahedral elements, the edge basis function associated with the i_{th} edge is given by

$$N_i^e = \left(L_i^e \nabla L_j^e - L_j^e \nabla L_i^e\right)/l_{ij}$$
$$L_i^e = \frac{1}{6V^e}\left(a_i^e + b_i^e x + c_i^e y + d_i^e z\right). \quad (24)$$

Further, L_k^e (k = 1, 2, 3, 4) are the basis node of basis functions associated with the four vertices of the tetrahedral, where a_i^e, b_i^e, c_i^e, and d_i^e are defined as in [9], and i_1 and i_2 denote the two vertices associated with the i_{th} edge and l_i^e is the length of the i_{th} edge.

In this paper, we will replace the traditional functions given in (24) by the multiscalets interpolation functions with multiplicity *r=3*

$$\begin{aligned}
W_{t1}^e &= \left(-3N_1^5 + 7N_1^4 - 4N_1^3\right)^e l_1^e,\\
W_{t2}^e &= \left(-3N_2^5 + 7N_2^4 - 4N_2^3\right)^e l_2^e,\\
W_{t3}^e &= \left(-3N_3^5 + 7N_3^4 - 4N_3^3\right)^e l_3^e,\\
W_{t4}^e &= \left(-3N_4^5 + 7N_4^4 - 4N_4^3\right)^e l_4^e\\
W_{t5}^e &= \left(-3N_5^5 + 7N_5^4 - 4N_5^3\right)^e l_5^e\\
W_{t6}^e &= \left(-3N_6^5 + 7N_6^4 - 4N_6^3\right)^e l_6^e
\end{aligned} \quad (25)$$

It can be demonstrated that W_t^e satisfies automatically the convergence condition.

Once the basis functions are determined, the electric (or magnetic) field within each element can be expanded as

$$E = \sum_{j=1}^{m} E_j^e W_{tj}^e, \quad (26)$$

where m is the number of interpolating points (depending on the order of basis functions) within each element (in this case *m=6*). Substituting (26) into (23) and applying Galerkin's method, the following matrix equation for each tetrahedron is derived.

$$\left\{\left[K^e\right] - k_0^2\left[M^e\right]\right\}\left(E^e\right) = -jk_0 Z_0\left(F^e\right), \quad (27)$$

where

$$\begin{aligned}
K_{ij}^e &= \frac{1}{\mu_r}\iiint_{V^e}\left(\nabla \times W_i^e\right)\cdot\left(\nabla \times W_j^e\right) d\Omega\\
M_{ij}^e &= \varepsilon_r \iiint_{V^e} W_i^e \cdot W_j^e \; d\Omega\\
F_i^e &= \iiint_{V^e} W_i^e J d\Omega.
\end{aligned} \quad (28)$$

Corresponding to all tetrahedral, a global matrix equation of the following form can be derived:

$$[A](E) = (F), \quad (29)$$

where

$$\begin{aligned}
[A] &= \sum_{e=1}^{M}\left(\left[K^e\right] - k_0^2\left[M^e\right]\right)\\
(E) &= \sum_{e=1}^{M}\left(E^e\right)\\
(F) &= -jk_0 Z_0 \sum_{e=1}^{M}\left(F^e\right),
\end{aligned} \quad (30)$$

and M is the total number of tetrahedral. The FEM mass matrix [A] is symmetric, positive with an order *n,* where *n* is the total number of edges in the whole domain Ω and (F) is an appropriate excitation vector which has non-zero elements only in the position of excitation edges.

The final matrix equation is of very large order but the corresponding square matrix is sparse. For that, we can use of appropriate iterative conjugate gradient (CG) techniques.

B. Boundaries conditions

Let us consider the unit cell in an infinite periodic structure, as shown in Figure 2; the interior volume, denoted here as V, is enclosed by four side surfaces: a top surface, and a bottom surface. It may contain arbitrary dielectric and conducting structures.

The four side surfaces S_{x1}; S_{x2}; S_{z1}, and S_{z2} are located at $x = 0$; $x = Dx$; z = 0, and z = Dz, respectively, where Dx and Dz are periodic lengths in the x and z directions. The top surface S_t is the interface between free-space and the unit cell region. The bottom surface S_b is usually a ground plane. It may also contain waveguide apertures S_w that provide excitation for the radiation case. In a general configuration, 4 kinds of boundaries conditions are involved. On the four side surfaces, periodic boundaries conditions are imposed, relating the fields on the opposite side surfaces. On the top surface, a periodic radiation boundary condition is imposed; it simulates the radiation towards the free space in the presence of an infinite array. If a waveguide is present in the structure, a waveguide port condition is imposed on S_w. Finally, on conducting surfaces, a perfectly electrically conducting (PEC) boundary condition is enforced explicitly as a homogeneous Dirichlet boundary condition.

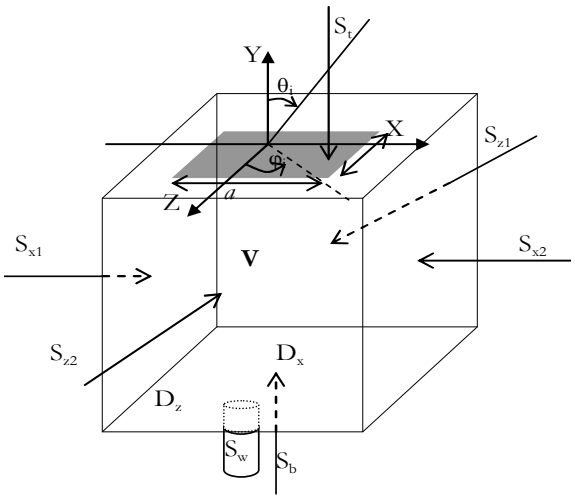

Fig. 2. The unit cell used for FEM calculations of periodic structures along with the locations of the various truncation boundaries where either absorbing or periodic boundaries conditions are imposed.

Periodic boundaries conditions can be derived directly from the Floquet theorem [13]. In accordance with the Floquet theorem, the electromagnetic fields inside and above the periodic media should satisfy

$$E(x+mD_x, z+nD_z) = E(x,z)e^{j(mk_{xi}D_x + nk_{zi}D_z)} \quad (31)$$

$$H(x+mD_x, z+nD_z) = H(x,z)e^{j(mk_{xi}D_x + nk_{zi}D_z)}, \quad (32)$$

where

$$k_{xi} = k_0 sin\theta_i cos\varphi_i \quad (33)$$

$$k_{zi} = k_0 sin\theta_i sin\varphi_i, \quad (34)$$

where (θ_i , φ_i) are the incident and scan angles. The periodicity forces the incident energy to propagate along certain directions. These propagation modes are defined analytically in the top surface S_t by the following equations:

$\Delta E_i - k_y^2 E_i = 0$ with $k_y = (\varepsilon_h \mu_h)^{1/2}\omega$ with h is the correspondent space area.

To facilitate the implementation of periodic boundaries conditions, identical surface meshes are created on the opposite side surfaces. Then, for each unknown E_i on one side surface, a corresponding unknown E_j is identified on the opposite surface which has the same relative position as E_i.

By applying the Floquet theorem (31), we obtain the following relationship between E_i and E_j:

$$E_j = E_i e^{j\psi_{ij}}, \quad (35)$$

where ψ_{ij} is a phase shift term given by

$$\psi_{ij}\begin{cases} k_{xi}D_x & \forall E_i \in S_{x1},\ E_j \in S_{x2} \\ k_{zi}D_z & \forall E_i \in S_{z1},\ E_j \in S_{z2} \\ k_{xi}D_x + k_{zi}D_z & \forall E_i \in S_{x1} \cap S_{z1},\ E_j \in S_{x2} \cap S_{z2} \end{cases} \quad (36)$$

In the matrix context, (35) is enforced explicitly as an inhomogeneous Dirichlet boundary condition. That's why, for each unknown pair (E_i;E_j): E_j is eliminated; the matrix entries associated with E_i are modified as plane is placed on S_t.

$$K_{il} = K_{il} + K_{jl}e^{j\psi_{ij}}, \quad (37)$$

For all $E_l \notin S_{x2} \cup S_{z2}$, and

$$K_{ik} = K_{ik} + K_{jl}e^{j(\psi_{ij} - \psi_{kl})}, \quad (38)$$

For all $E_l \in S_{x2} \cup S_{z2}$ which is related to E_k by phase shift $\psi_{kl;}$ and finally, the right-hand-side (RHS) vector entry associated with E_i is modified as

$$F_i = F_i + F_j e^{j\psi_{ij}}, \quad (39)$$

The function (23) contains a surface integral term over the top surface S_t with a form given by

$$S(E) = \iint_{S_t} \left[\frac{\gamma_e}{2}(\hat{n}\times E)\cdot(\hat{n}\times E) + E\cdot U \right] dS, \quad (40)$$

where U which may be expressed as

$$U = \frac{1}{\mu_r}\hat{n}(\nabla \times E) + \gamma_e \hat{n}\times(\hat{n}\times E)\cdot \quad (41)$$

γ_e is known parameter given by $\gamma_e = -\frac{jk_0\mu_r}{\eta}$, with $\eta = \sqrt{\mu_r/\varepsilon_r}$.

IV. REDUCTION MESHING

Our refinement scheme described in Fig. 3 and the coarse grid tetrahedron is split into four tetrahedral which are similar to their parent and one different tetrahedral in the center.

Hence, our refinement procedure results in only two classes of similar tetrahedral, assuming that mesh quality will never deteriorate. The idea is to eliminate four tetrahedral to surround with the cubic element and to leave only the central tetrahedral.

This technique of meshing used to adapt FEM method with other numerical method like the TLM method, iterative method etc. in case of a hybridization technique, where we convert the value of every edge elements to at point (Fig. 4. d). With this technique, we can superpose a

resulting matrix of these numerical methods with our of FEM matrix to obtain the value in inner waveguide.

In the next figure, we present the different steps to get our appropriate and desired meshing based on the strategy given by Fig. 3.

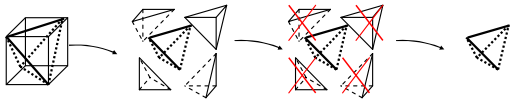

Fig. 3. Element Hexahedral subdivided into five tetrahedral with elimination of the secondary tetrahedral.

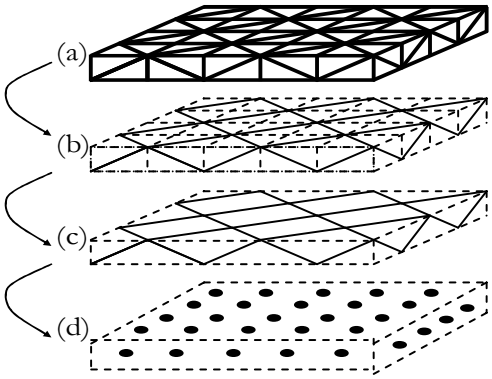

Fig. 4. A waveguide devised in tetrahedral elements where only a center tetrahedral is needed.

The next table presents the efficiency technique to reduce the size of a regular structure, and presents the reduction report between the typical meshing and reduction meshing and another table that presents gain obtained in time considering proper characteristics of the used machine.

Table 1: Reduction report between typical meshing and reduction meshing

Cells Number	Typical Meshes	Reduction Meshes	Reduction Report
16×1×16	2433 edges	1056 edges	≈ 44%
32×1×32	9473 edges	4160 edges	
64×1×64	37377 edges	16512 edges	
128×1×128	148481 edges	65792 edges	

Table 2: Time report between typical and new reduction meshing for different size matrix with a CPU 3 GHz and 4 GB of memory

CPU	Memory	Number of Cells	Time (sec) for 10 iterations		Time (sec) between typical and new meshing
			Typical Meshing	New Meshing	
3 GHz	4Go	16×1×16	16	1,4	11,42
		32×1×32	96	10,2	9,41
		64×1×64	868	97	8,95
		128×1×128	9223	1321	6,98

This purpose will greatly simplify the electromagnetic analysis of the CPU time of simulation by enabling the characterization of the electromagnetic interaction with the entire structure.

V. NUMERICAL RESULTS

This section contains a series of examples that validate the MSRM-FEM formulation compared with analytic and reference results. Our strategy is based on a unit cell divided on $32\Delta x \times 4\Delta y \times 32\Delta z$ elements. All given examples were studied and carried out with a gain of 4 in memory consumption.

In this part, we consider the finite element analysis in the two-dimensional xz-plane. Although not a physically realistic configuration, the infinite array model provides a reasonably good approximation to the performance of the interior elements in a large finite array. Here, we suppose that this finite unit cell, the patch characterized by its infinite thin thickness is inserted between two dielectric layers that have the same dielectric permittivity.

To show that the periodic boundaries conditions and periodic radiation boundaries conditions are correctly modeling the field behaviour, a simple example is tested. We use a 20 cm thick uniform dielectric layer composed of dielectric with relative permittivity ε_r=2.2-j and backed with a ground plane. The analysis takes into account different oblique incidences. It proves clearly that the reflection coefficient is independent of both angle and polarization of incidence.

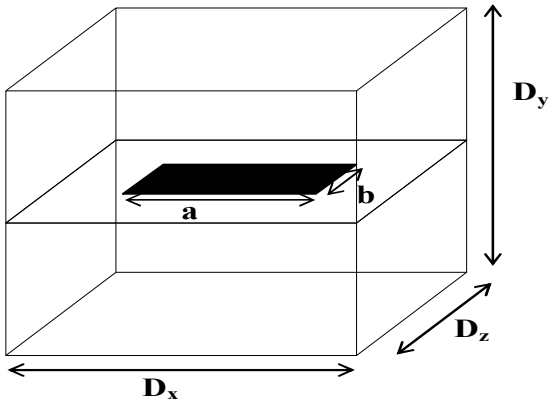

Fig. 5. Rectangular patch unit cell laid between two dielectric.

Here, for an incident plane wave with an incident angle θ = 60°, the TE and the TM refection coefficients, shown in Fig. 5, are calculated over the frequency band 0.1 to 0.5 GHz. In the FEM, the unit cell is modeled as a 20×20×20cm homogeneous dielectric box with a ground plane placed on its bottom surface. Good agreement between our MSRM-FEM results and the analytical solutions has to validate considered in the periodic boundary conditions and the periodic radiation boundary conditions.

The dielectric slab is backed by a ground plane. The reflection coefficient should always have magnitude of 1 because all the energy shall be reflected. In our example, it has a few differences with the analytic results. This is due to the intrinsic properties of the used dielectric characterized by its proper properties. In another way, this is not a perfect dielectric characterized by a complex permittivity (ε_r=2.2-j).

The next example is the reflection due to an incident upon a plane wave onto a frequency selective surface structure. The unit cell presented in Fig. 5 is a rectangular patch laid between two dielectric with 2-mm-thick with a complex permittivity ε_r=2.2-j, and following geometric dimensions D_x=D_z=10.0 mm, D_y=2.0 mm, a=2.5mm and b=5mm.

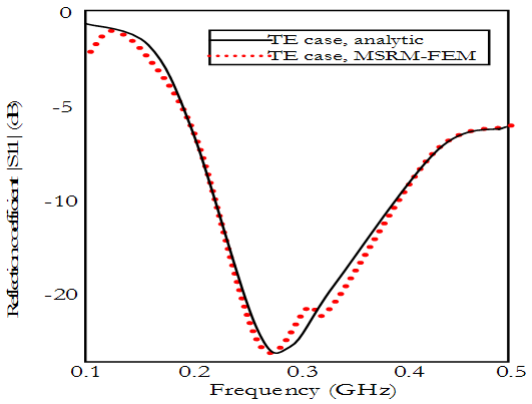

(a)

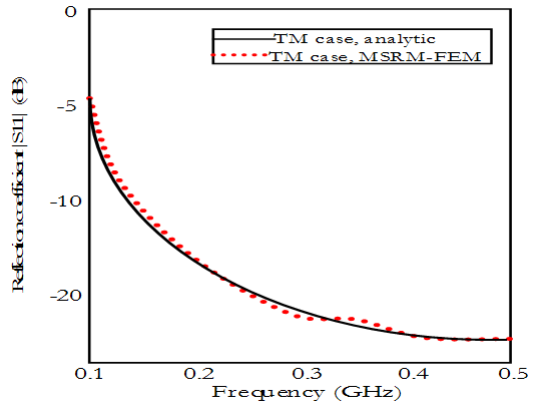

(b)

Fig. 6. Reflection coefficient for the 20-cm-thik uniform layer (ε_r=2.2) backed with ground plane plate at θ=60° and φ =0 for (a) TE, (b) TM.

The normalised power reflection coefficient for an oblique incidence is shown in Fig. 7. It is compared with the analytic results given by the advanced design system (ADS 2004) simulator.

The second example (Fig. 8) presents the normalised transmitted power coefficient for a real permittivity (ε_r=4) and following geometric dimensions D_x=50.0 mm, D_z=4.0 mm, a= D_x/2 and b= D_z. The unite cell is presented in Figure 5. This 3-D structure is simulated using MSRM-FEM FORTRAN code, and compared with FDTD reference solution [13].

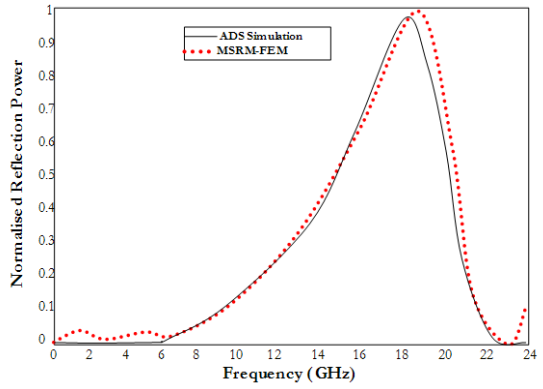

Fig. 7. The normalised power reflection coefficient with side view unit cell, for an oblique incidence.

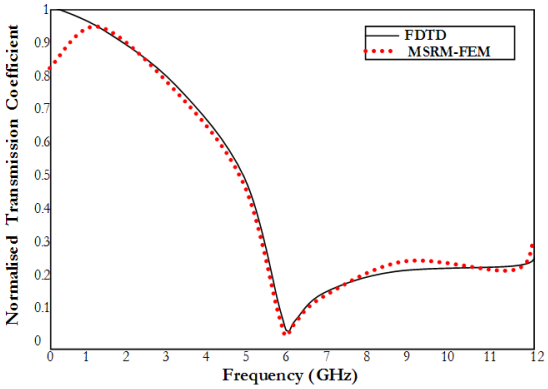

Fig. 8. The normalised power transmission coefficient with side view unit cell, for an oblique incidence (θ_i, φ_i)=(90°,0°).

The incident angle (*theta* = 90 degrees) shows a grazing incidence. Here, very high absorption of energy was shown at the resonant frequency 6 GHz.

Figure 9 shows the normalised transmission power as a function of the frequency, for several values of *a*. The computed values are indicated with symbols, and intermediate values have been obtained using multiscalets interpolation.

In all cases, a significant absorption band is observed. In addition, the critical frequency (frequency in which value attains its minimum) decreases as the ratio a/*D* increases.

For a real permittivity (ε_r=10.2) and following geometric dimensions D_x= D_z=10mm, D_y=2.0 mm, *a*=*b*=1.0, 4.0 and 8.0 mm.

Figure 10 presents the normalised transmission power as a function of the frequency, for several values of incident angle θ. These results show that the critical frequency value depends very weakly on the incidence angle.

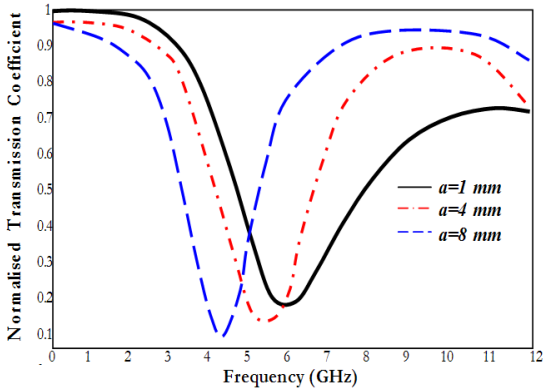

Fig. 9. The normalised power transmission coefficient for various values of the plat's size: for an oblique incidence (θ_i, φ_i)=(90°,0°).

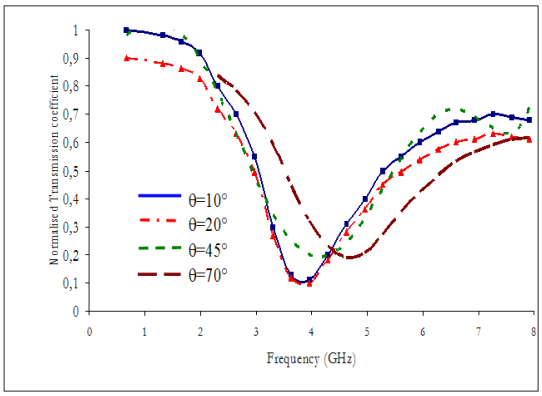

Fig. 10. The normalised transmission coefficient as a function of the incident frequency, for various values of incident angle: θ =10°, 20°, 45° and 70°. The period D_x=D_z =10.0 mm, D_y=2.0 mm and the plate's size *a* are kept fixed *a* = 8.0 mm and ε_r=10.2.

VI. CONCLUSION

In our paper, a new FEM analysis of infinite periodic structures described by MSRM-FEM is presented. The theoretical basis of FEM theory, combined with the Floquet theorem and the integral equation formulation analysed with new technical meshing strategy is presented. Higher-order multiscalets vector basis functions are used to expand electromagnetic fields. Numerical results have demonstrated the efficiency and

accuracy of using higher order multiscalets vector basis functions.

The reduction meshing (RM) based technique is combined with FEM to reduce the size of resulting matrix, consequently, minimization of memory and time consumption, 7~11 in time speed compared with typical meshing.

The FEM feed modeling is, also, discussed in detail in radiation problem cases. The validity and versatility of the FEM formulation have been demonstrated through numerical results compared with analytic and published simulations.

REFERENCES

[1] R. Mittra, C. H. Chan, and T. Cwik, "Techniques for analyzing frequency selective surfaces," *Proc. IEEE,* vol. 76, pp. 1593–1615, Dec. 1988.

[2] N. Amitay, V. Galindo, and C. P. Wu, *Theory and Analysis of Phased Array Antennas*, New York: Wiley, 1972.

[3] Daniel G. Swanson, Jr and Wolfgang J. R. , *Microwave Circuit Modeling Using Electromagnetic Field Simulation,* Artech House, Inc., 2003.

[4] J. L. Volakis, T. F. Eibert, D. S. Filipovic, Y. E. Erdemli, and E. Topsakal, "Hybrid finite element methods for array and FSS analysis using multiresolution elements and fast integral techniques," *Electromagn.*, vol. 22, pp. 297-313, May-Jun 2002.

[5] J. M. Jin and J. L. Volakis, "Scattering and radiation analysis of three-dimensional cavity array via a hybrid finite-element method," *IEEE Trans. Antennas Propagat.,* vol. 41, pp. 1580-1586, Nov. 1993.

[6] G. Pan, *Wavelet in Electromagnetics and Device Modeling,* Hoboken, NJ: Wiley, 2003.

[7] Y. Zhu and A.C Cangellary "Hierarchical Multilevel Potential Preconditioner for Fast Finite-Element Analysis of Microwave Devices," *IEEE Trans. Microwave Theory and Tech.,* vol. 50, no. 8, pp. 1984-1989, Aug. 2002.

[8] W. Miller, "Introduction to the Mathematics of Wavelets," *Lecture Notes and Background Materials for Math 5467*, May 7, 2004.

[9] J. Jin, *The Finite Element Method in Electromagnetics,* New York , Wiley 2002.

[10] M. L. Barton and Z. Cendes "New Vector Finite Element for Three-Dimensional Magnetic Field Computation," *Journal. Appl. Phys.,* vol. 61, no. 8, pp. 3919-3921, April 1987.

[11] Y. Zhu and R. Lee, "TVFEM Analysis of Periodic Structures for Radiation and Scattering," *Progress In Electromagnetics Research,* vol. 25, pp. 1–22, 2000.

[12] V. Hill, O. Farle and R. Dyczij-Edlinger "A Stabilized Multilevel Vector Finite Element Solver for Time-harmonic Electromagnetic Waves," *IEEE Transaction on Magnetic.,* vol. 39, no. 39, pp. 1203-1207, May 2003.

[13] E. A. Navarro, B. Gimeno, and J.L. Cruz, "Modelling of periodic structures using the finite difference time domain method combined with the Floquet theorem," *Electronics Letters,* vol. 29, no.5, March 1993.

Adel Ben Ali received the degree in electronic engineering in 1999 and the M.Sc. degree in communications systems from ELManar University- National Engineering School Tunis, Tunisia, in 2002. He is currently working toward the Ph.D. degree in electrical engineering. His research interests include analysis of microwave structures, microwave integrated circuits by finite element method

El Amjed Hajlaoui received the degree in electronic engineering in 2001 and the M.Sc. degree and Ph.D. in communications systems from ELManar University- National Engineering School Tunis, Tunisia, respectively, in 2003 and 2008. His research interests include multilayered structures, microwave integrated circuits, and quasi-optic structures.

Ali Gharsallah received the degrees in radio-electrical engineering from the Ecole Supérieure de Télécommunication de Tunis in 1986 and the Ph.D. degree in 1994 from the Ecole d'Ingénieurs de Tunis. Since 1991, he was with the department of Physics at the Faculty of Sciences, Tunis. His current research interests include antennas, multilayered structures and microwave integrated circuits.